


Article

Large-Signal Stabilization Method for Islanded DC Microgrids Considering Battery and Supercapacitor Hybrid Energy Storage Systems

Xinbo Liu , Yongbing Suo, Xiaotong Song, Jinghua Zhou and Yaxin Qu

School of Electrical and Control Engineering, North China University of Technology, Beijing 100144, China

* Correspondence: liuxinbo@ncut.edu.cn

Abstract: Islanded DC microgrids composed of distributed generators (DGs), constant power loads (CPLs), parallel converters, batteries and supercapacitors (SCs) are typical nonlinear systems, and guaranteeing large-signal stability is a key issue. In this paper, the nonlinear model of a DC microgrid with a hybrid energy storage system (HESS) is established, and large-signal stability criteria are obtained. The HESS consists of batteries and SCs. The derived criteria reveal the influences of the filter parameters, CPL power, DG power and the proportional control parameters of the battery converter and the SC converter on the system large-signal stability. Furthermore, important large-signal stabilization methods for regulating the HESS converter's control parameters can easily achieve the large-signal stabilization of islanded DC microgrids without extra equipment. The paper is summarized as follows: First, the topology of and control strategy for a DC microgrid with an HESS and CPLs are proposed. Then, according to the characteristics of the HESS, the DGs and the CPLs, the system is equivalently simplified. Finally, the nonlinear model and large-signal stability criteria are both derived using the mixed potential theory, and a large-signal stabilization design method for the HESS converter's control parameters is proposed. The experimental and simulation results show the effectiveness of the proposed large-signal stabilization method.

Keywords: large-signal stability; islanded DC microgrids; hybrid energy storage system (HESS); mixed potential function; constant power loads (CPLs); parallel converters



Citation: Liu, X.; Suo, Y.; Song, X.; Zhou, J.; Qu, Y. Large-Signal Stabilization Method for Islanded DC Microgrids Considering Battery and Supercapacitor Hybrid Energy Storage Systems. *Electronics* **2022**, *11*, 2823. <https://doi.org/10.3390/electronics11182823>

Academic Editors: Ayan Mallik and Irfan Ahmad Khan

Received: 6 August 2022

Accepted: 5 September 2022

Published: 7 September 2022

Publisher's Note: MDPI stays neutral with regard to jurisdictional claims in published maps and institutional affiliations.



Copyright: © 2022 by the authors. Licensee MDPI, Basel, Switzerland. This article is an open access article distributed under the terms and conditions of the Creative Commons Attribution (CC BY) license (<https://creativecommons.org/licenses/by/4.0/>).

1. Introduction

In DC microgrids, reactive power, harmonics, frequency and phase are not involved, as only DC voltage is included and considered. DC microgrids integrate distributed generators (DGs), different loads, energy storage systems (ESSs) and various converters and are increasingly utilized [1–3]. Unfortunately, the inertia of islanded DC microgrids is very small, and the DC bus voltage is extremely sensitive to disturbances. Furthermore, large power variations of DGs and loads commonly exist in DC microgrids; consequently, maintaining DC bus voltage stability becomes the key issue [4–8].

The ESS is used to eliminate the DC bus voltage fluctuations of DC microgrids, and the appropriate control of the ESS could enhance the system stability [9–11]. Batteries are widely adopted in ESSs; however, frequent charging and discharging processes significantly decrease their work life. Consequently, DC microgrids mostly use hybrid energy storage systems that combine high-energy-density batteries with high-power-density supercapacitors [12,13]. The batteries absorb or release low-frequency-power fluctuations, while high-frequency-power fluctuations are stabilized by the SC. The parallel converters of batteries and SCs introduce great difficulties for HESS control and DC microgrids' stability [14]. Furthermore, research on HESSs mostly focuses on control strategies and power-allocation optimizations. Intelligent algorithms such as PI control, model predictive control, sliding mode control and fuzzy control have been widely used in HESS converters [15]. The low-pass-filtering method and wavelet packet decomposition method are utilized to achieve

power allocation [16]. However, there are few studies about the quantitative stability analysis of HESS converters' control parameters on islanded DC microgrids.

On the other hand, in DC microgrids, most of the loads connected to the DC bus through closed-loop control converters are equivalent to constant power loads [17]. The negative incremental impedances of the CPLs significantly deteriorate system stability during large disturbances, and the CPLs' influences on islanded DC microgrids is extremely strong [18,19]. Consequently, many methods have been proposed to compensate the characteristics of the CPLs.

In [20,21], active or passive damping is added to the source converters to compensate the CPLs. In order to increase the system damping, the authors of [22] increase the DC bus capacitance, while the authors of [23] propose the virtual impedance method. The authors of [24] and [25] propose a sliding-mode duty-ratio controller, backstepping and a nonlinear disturbance observer for a DC-DC converter with CPLs. However, these studies mainly focus on improving system stability based on specific control or analysis methods and are applicable for single DC-DC converters feeding CPLs. The authors of [26] propose a control method based on DC current feedforward, and the authors of [27] present a Takagi–Sugeno fuzzy-based model predictive control strategy to improve the stability of DC microgrid systems under the influence of CPLs. Unfortunately, there are few references that consider the negative influences of the CPLs and simultaneously also consider the positive influences of HESS converters' control parameters.

Generally speaking, small-signal stabilization and large-signal stabilization are the main methods for the stability analysis of DC microgrids [28]. Based on linearization techniques at steady-state equilibrium operating points, small-signal stability guarantees DC bus voltage stability during small disturbances and is not suitable for large disturbances [29,30]. Unfortunately, the DC microgrid is a typical nonlinear system, and steady-state equilibrium operating points are constantly changing; consequently, small-signal stability methods cannot ensure DC microgrid stability under large power variations of DGs and loads [31,32].

Large-signal stability analysis usually uses the Lyapunov function [33,34]. However, constructing Lyapunov functions is very difficult. Furthermore, mixed potential theory is proposed to build Lyapunov-type functions and derive stability criteria [35]. Refs. [19,36] present a mixed potential function for cascaded BUCK/BOOST converters and analyze the control parameters' influences on system stability. Reference [37] proposes a mixed potential function of DC/DC bidirectional converters and achieves proper controller limiting to improve large-signal stability. Refs. [38,39] study the large-signal stability of DC microgrids considering battery energy storage systems. Additionally, voltage-controlled converters and current-controlled converters are both taken into account in [39]. In [40,41], a large-signal stability criterion for DC microgrids is derived using a Lyapunov function, and the stable operation range and maximum load power of the system are analyzed. Reference [42] proposes a large-signal stability criterion for DC microgrids with multiple converters and analyzes the relationship between stable operation range and load power. Reference [43] improves the stability of DC microgrids considering fault and distributed energy power allocation. Unfortunately, it is not easy to obtain the large-signal models of complicated systems using mixed potential functions. Consequently, the large-signal stability analysis of DC microgrids integrating an HESS, CPLs and DGs is rarely reported, and simultaneously, the stability influences of the control parameters and the powers are not considered.

This paper attempts to fill the gap through the following research study, and the contributions are as follows:

- (1) The topological structure of and control strategy for islanded DC microgrids containing CPLs, DGs and an HESS are proposed. A nonlinear model of the system is obtained. Based on the mixed potential function theory, a large-signal model and a large-signal stability criterion for DC microgrids are obtained;

- (2) The presented large-signal stability criterion reveals the relationships among the filtering parameters, DG power, CPL power, the proportional control parameter (k_{ip1}) of the inner current loop for the battery converter, the proportional control parameter (k_{vp2}) of the outer power loop for the SC converter and the stability of the islanded DC microgrids. Moreover, simultaneously, important large-signal stabilization design methods for the HESS converter's control parameters for DC microgrids are provided;
- (3) Regulating the proportional control parameter (k_{ip1}) of the inner current loop for the battery converter and the proportional control parameter (k_{vp2}) of the outer power loop for the SC converter can optimize a control strategy for islanded DC microgrids and enhance system stability without extra equipment.

2. Modeling of and Control Strategy for DC Microgrids

Typical islanded DC microgrids are constituted of DGs, CPLs and an HESS, as shown in Figure 1. Most HESSs are connected to the DC bus through bidirectional BUCK/BOOST converters. Closed-loop-controlled motors and other loads are considered CPLs. DGs are equivalent to the current source. The simplified structure of an islanded DC microgrid with an HESS, CPLs and parallel converters is shown in Figure 2.

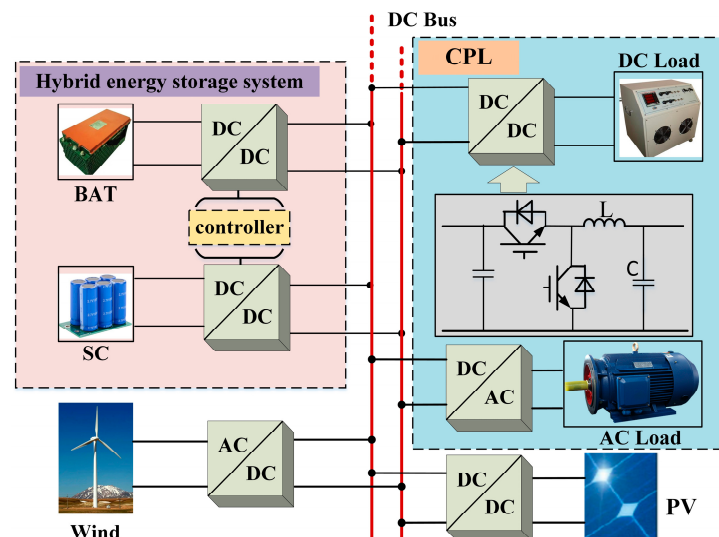


Figure 1. Structure of typical islanded DC microgrid.

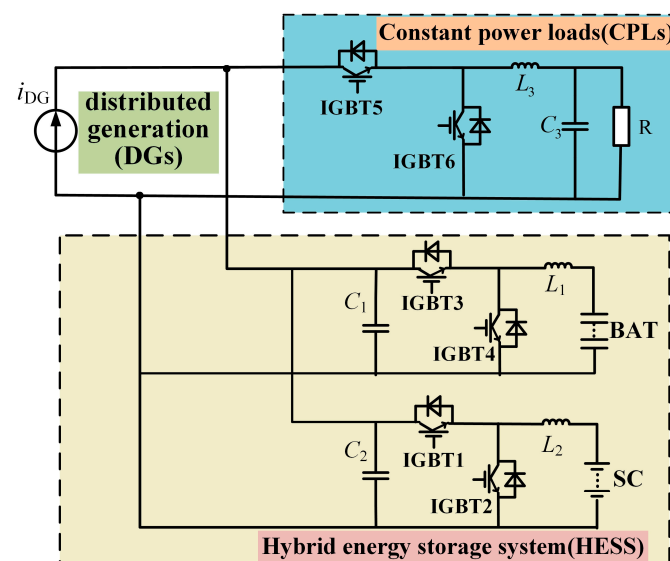


Figure 2. Simplified structure of islanded DC microgrid with HESS, CPLs and DGs.

2.1. Modeling

The bidirectional DC/DC converter of an HESS can be operated in buck mode and boost mode. When the HESS absorbs energy, the DC/DC converter works in buck mode, as shown in Figure 3. When the HESS outputs energy, the DC/DC converter works in boost mode, as shown in Figure 4.

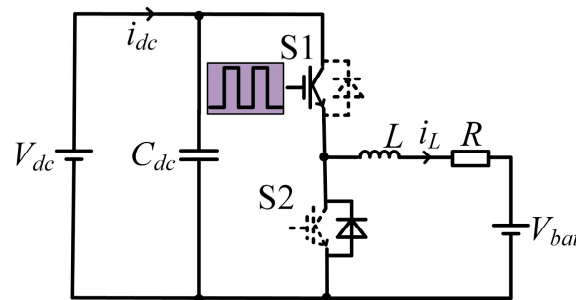


Figure 3. Principle diagram of bidirectional DC/DC converter working in buck mode.

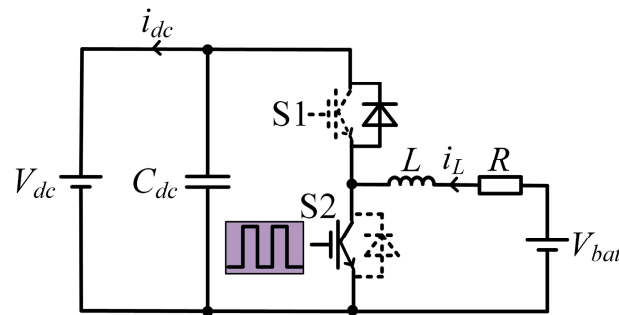


Figure 4. Principle diagram of bidirectional DC/DC converter working in boost mode.

The bidirectional DC/DC converter of the battery is described as:

$$v_{dc} = \alpha v_{bat} - \alpha R i_L - \alpha L \frac{di_L}{dt} \quad (1)$$

In (1), v_{dc} is the DC bus voltage, v_{bat} is the battery voltage, i_L is the inductor current, R is the battery equivalent resistance, and α is the battery charging and discharging factor.

Moreover, the bidirectional DC/DC converter of batteries adopts an inductor current inner loop and a DC bus voltage outer loop; therefore, the battery and DC/DC converter are equivalent to a voltage source in series with the equivalent resistor and inductor, as shown in Figure 5.

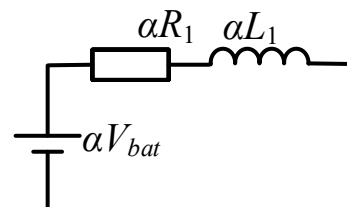


Figure 5. Equivalent model of battery and bidirectional DC/DC converter.

The bidirectional DC/DC converter of a SC utilizes a power outer loop and a current inner loop; consequently, the SC and the DC/DC converter are equivalent to a controlled power source whose power is P_{sc} , as shown in Figure 6.

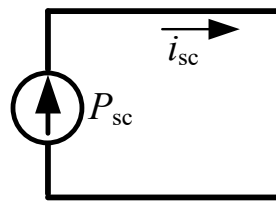


Figure 6. Equivalent model of SC and bidirectional DC/DC converter.

The power relationship of the SC and DC/DC converter is:

$$i_{sc}v_{dc} = i_{SC}v_{SC} = P_{sc} \quad (2)$$

In (2), i_{sc} is the output current of the DC/DC converter, and v_{SC} and i_{SC} are the voltage and current of the SC, respectively.

In a DC microgrid, the loads are connected in parallel to the DC bus through converters. Due to the closed-loop control, when the DC bus voltage increases, the input current of these loads decreases, and the power remains constant. These loads are regarded as CPLs, and the voltage–current characteristics of the CPLs are shown in (3). The equivalent model of the CPLs is shown in Figure 7.

$$i_{CPL} = \frac{P_{CPL}}{v_{CPL}} \quad (3)$$

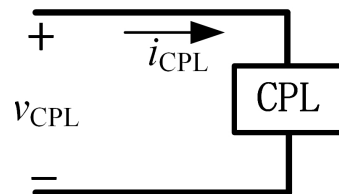


Figure 7. Equivalent model of CPLs.

In (3), i_{CPL} , P_{CPL} and v_{CPL} are the input current, the power and the input voltage of the CPLs, respectively.

DGs usually adopt the constant current mode and are equivalent to a power source whose power is P_{DG} .

Consequently, the nonlinear model of a DC microgrid with an HESS is established as shown in Figure 8.

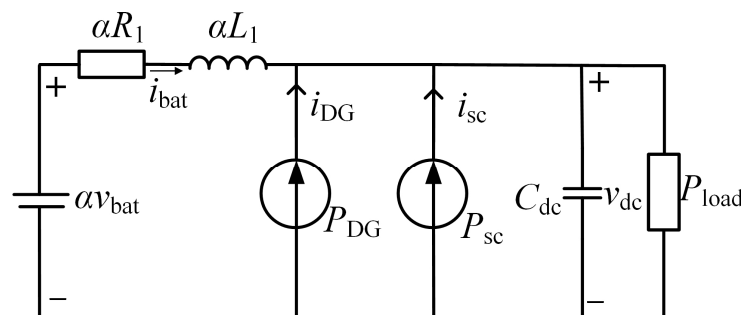


Figure 8. Nonlinear model of a DC microgrid.

In Figure 8, v_{bat} is the battery voltage, i_{bat} is the battery current, R_1 is the equivalent internal resistance of the battery, L_1 is the inductance of the bidirectional DC/DC converter, and DG and SC are equivalent to the power sources whose powers are P_{DG} and P_{sc} , respectively. The output currents of DGs and the SC are i_{DG} and i_{sc} , respectively. C_{dc} is the filter capacitor, and its voltage is v_{dc} , while P_{load} is the power of the CPLs.

2.2. Control Strategy

According to the power of DGs and CPLs, the reference power of the HESS is derived. The power of the HESS is divided into high-frequency power and low-frequency power using a low-pass filter (LPF), as shown in Figure 9. The power relationships are:

$$P_{DG} - P_{load} = P_{bat-ref} + P_{sc-ref} \quad (4)$$

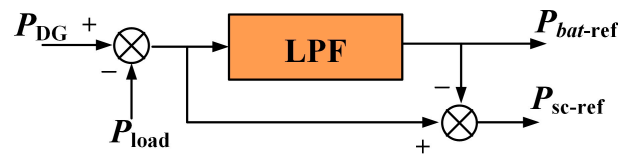


Figure 9. Control block diagram of low-pass filter (LPF).

In (4), $P_{bat-ref}$ and P_{sc-ref} are the reference powers for the battery and for the supercapacitor, respectively.

The battery converter maintains constant DC bus voltage. Therefore, the battery converter adopts the outer voltage loop and the inner current loop to control the charging or discharging. The voltage outer loop calculates the reference value for the current inner loop control. The current inner loop makes the actual current (I_{bat}) of the battery unit track the current reference value ($I_{bat-ref}$) through the PI controller to eliminate the steady-state error of current tracking. Finally, the complementary control signals are output by the PWM generator.

On the other hand, the supercapacitor (SC) converter utilizes the outer power loop and inner current loop. The power outer loop calculates the reference value of the current inner control loop. The current inner loop makes the actual SC current (I_{sc}) track the current reference value (I_{sc-ref}) through the PI controller to eliminate the steady-state error of current tracking. Finally, the complementary control signals are output by the PWM generator.

The control strategy for HESS converters is shown in Figure 10.

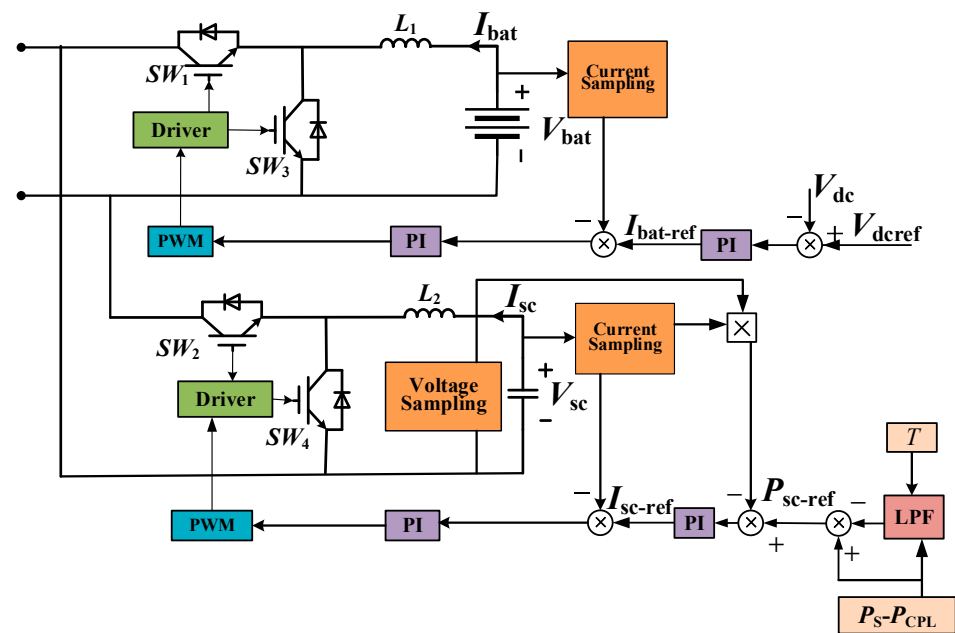


Figure 10. Control block diagram of HESS converters.

In Figure 10, V_{ref} is the reference DC bus voltage, $I_{bat-ref}$ is the reference current of the battery converter, and V_{dc} and I_{bat} are the actual output voltage and current of the battery converter. $P_{bat-ref}$ and P_{sc-ref} are the reference power for the battery and for the

supercapacitor, respectively. The LPF adopts the first-order low-pass filter, and its transfer function is shown in (5):

$$H(s) = \frac{1}{Ts + 1} \quad (5)$$

According to (4) and (5), the reference power of the battery and the SC are calculated, respectively, and shown as:

$$P_{bat-ref} = \frac{1}{Ts + 1}(P_{DG} - P_{load}) = \frac{1}{Ts + 1}P_{HESS} \quad (6)$$

$$P_{sc-ref} = \frac{Ts}{Ts + 1}(P_{DG} - P_{load}) = \frac{Ts}{Ts + 1}P_{HESS} \quad (7)$$

In (6) and (7), P_{HESS} is the total reference power of the HESS. Based on (6) and (7), (8) and (9) are derived and shown as:

$$T \frac{dP_{bat-ref}(t)}{dt} + P_{bat-ref}(t) = P_{HESS}(t) \quad (8)$$

$$T \frac{dP_{bat-ref}(k+1) - dP_{bat-ref}(k)}{T_s} + P_{bat-ref}(k+1) = P_{HESS}(k+1) \quad (9)$$

In (8) and (9), T is the low-pass-filtering coefficient, and T_s is the sampling period. $P_{bat-ref}(k+1)$ is the battery reference power for the next sampling period, and $P_{sc-ref}(k+1)$ is the SC reference power for the next sampling period.

Based on (6), (8) and (9), $P_{bat-ref}(k+1)$ are obtained and shown as:

$$P_{bat-ref}(k+1) = \frac{T}{T + T_s}P_{bat-ref}(k) + \frac{T_s}{T + T_s}P_{HESS}(k+1) \quad (10)$$

Similarly, $P_{sc-ref}(k+1)$ are obtained on the basis of (7)–(9), and the derivation process is as follows:

$$T \frac{dP_{sc-ref}(t)}{dt} + P_{sc-ref}(t) = T \frac{dP_{HESS}(t)}{dt} \quad (11)$$

$$T \frac{dP_{sc-ref}(k+1) - dP_{sc-ref}(k)}{T_s} + P_{sc-ref}(k+1) = T \frac{dP_{HESS}(k+1) - dP_{HESS}(k)}{T_s} \quad (12)$$

$$P_{sc-ref}(k+1) = \frac{T}{T + T_s}(P_{sc-ref}(k) + P_{HESS}(k+1) - P_{HESS}(k)) \quad (13)$$

In (13), when $P_{HESS}(k+1) - P_{HESS}(k) = \Delta P_{HESS}$, the following is obtained.

$$P_{sc-ref}(k+1) = \frac{T}{T + T_s}(P_{sc-ref}(k) + \Delta P_{HESS}) \quad (14)$$

3. Large-Signal Stabilization Method

The mixed potential function is widely used in nonlinear systems containing inductance, capacitance, resistance and negative-impedance characteristic components. Compared with other stability analysis methods, the mixed potential function derives the quantitative stability criterion. Mixed potential function P is expressed as:

$$P(i, v) = -A(i) + B(v) + (i, \gamma v - \alpha) \quad (15)$$

where $A(i)$ is the current potential function, $B(v)$ is a voltage potential function and $(i, \gamma v - \alpha)$ varies with the system topology.

The general mixed potential function model is established as follows:

- (1) The potential function of non-energy storage components in the system is obtained;
- (2) The energy absorbed by the capacitor element in the system is calculated;
- (3) The formulas obtained are written in standard form.

For the established mixed potential function, (16) is used to verify its accuracy:

$$\begin{cases} L \frac{di_p}{dt} = \frac{\partial P(i,v)}{\partial i_p} \\ C \frac{dv_\sigma}{dt} = -\frac{\partial P(i,v)}{\partial v_\sigma} \end{cases} \quad (16)$$

In (16), i_p and v_σ are the current and voltage variables of the mixed potential function.

The third stability theory of mixed potential functions is often used to analyze the large-signal stability. The following are derived and shown as:

$$A_{ii}(i) = \frac{\partial^2 A(i)}{\partial i^2} \quad (17)$$

$$B_{vv}(v) = \frac{\partial^2 B(v)}{\partial v^2} \quad (18)$$

In (17), $A_{ii}(i)$ is the second-order partial derivative of the current potential function to the current variable, and in (18), $B_{vv}(v)$ is the second-order partial derivative of the voltage potential function to the voltage.

If the system satisfies:

$$\mu_1 + \mu_2 \geq \delta, \delta > 0 \quad (19)$$

In (19), μ_1 is the minimum eigenvalue of matrix $L^{-1/2}A_{ii}(i)L^{-1/2}$, and μ_2 is the minimum eigenvalue of matrix $C^{-1/2}B_{vv}(v)C^{-1/2}$.

Simultaneously, when $\|i\| + \|v\| \rightarrow \infty$, if the system satisfies:

$$P^*(i,v) = \frac{\mu_1 - \mu_2}{2}P(i,v) + \frac{1}{2}(P_i, L^{-1}P_i) + \frac{1}{2}(P_v, C^{-1}P_v) \rightarrow \infty \quad (20)$$

There is a convergence region that makes the system trajectory asymptotically converge to the steady-state equilibrium point.

Large-Signal Stabilization Method for DC Microgrids with HESS

On the basis of the simplified model of the HESS DC microgrid in Figure 8, the large-signal model of the system is established using the mixed potential function.

The current potential function of the battery equivalent model and bidirectional DC/DC converter is:

$$P_i = \alpha v_{bat} i_{bat} - \frac{1}{2} \alpha i_{bat}^2 R_1 \quad (21)$$

The voltage potential functions for the equivalent models of the DGs and the SC are:

$$P_v = P_{DG} - \int_0^{v_{dc}} \frac{P_{DG}}{v} dv + P_{sc} - \int_0^{v_{dc}} \frac{P_{sc}}{v} dv \quad (22)$$

The voltage potential function for the CPLs is:

$$P_v = -P_{load} + \int_0^{v_{dc}} \frac{P_{load}}{v} dv \quad (23)$$

The energy stored on capacitor C_{dc} is:

$$P_E = v_{dc} \left(\frac{P_{load}}{v_{dc}} - \frac{P_{DG}}{v_{dc}} - \frac{P_{sc}}{v_{dc}} - i_{bat} \right) \quad (24)$$

Based on (21) to (24), the mixed potential function of a DC microgrid is expressed as:

$$P(i, v) = \alpha v_{bat} i_{bat} - \frac{1}{2} \alpha i_{bat}^2 R_1 - \int_0^{v_{dc}} \frac{P_{DG}}{v} dv - \int_0^{v_{dc}} \frac{P_{sc}}{v} dv + \int_0^{v_{dc}} \frac{P_{load}}{v} dv - v_{dc} i_{bat} \quad (25)$$

The current potential function and voltage potential function in (25) are shown as:

$$A(i) = \begin{bmatrix} -\alpha v_{bat} i_{bat} + \frac{1}{2} \alpha i_{bat}^2 R_1 & 0 \\ 0 & 0 \end{bmatrix} \quad (26)$$

$$B(v) = \begin{bmatrix} -\int_0^{v_{dc}} \frac{P_{DG}}{v} dv - \int_0^{v_{dc}} \frac{P_{sc}}{v} dv + \int_0^{v_{dc}} \frac{P_{load}}{v} dv & 0 \\ 0 & 0 \end{bmatrix} \quad (27)$$

Equation (16) is applied to verify the verification of the mixed potential function model in (25):

$$\begin{cases} \frac{\partial P(i, v)}{\partial i_{bat}} = \alpha v_{bat} - i_{bat} R_1 - v_{dc} = \alpha L \frac{di_{bat}}{dt} \\ \frac{\partial P(i, v)}{\partial v_{dc}} = -\left(\frac{P_{DG}}{v_{dc}} + i_{bat} + \frac{P_{sc}}{v_{bat}} - \frac{P_{load}}{v_{bat}}\right) = -C \frac{dv_{dc}}{dt} \end{cases} \quad (28)$$

Obviously, (28) and (16) are consistent. Thus, the mixed potential function in (25), the voltage potential function and the current potential function are correct.

Based on (25), the large-signal stability criterion for DC microgrids is derived. Firstly, the quadratic partial derivatives of the current potential function and the voltage potential function are derived separately and shown as:

$$A_{ii} = \begin{bmatrix} -\frac{\partial \alpha v_{bat}}{\partial i_{bat}} + \alpha R_1 & 0 \\ 0 & 0 \end{bmatrix} \quad (29)$$

$$B_{vv} = \begin{bmatrix} \frac{P_{DG}}{v_{dc}^2} + \frac{\partial i_{sc}}{\partial v_{dc}} - \frac{P_{load}}{v_{dc}^2} & 0 \\ 0 & 0 \end{bmatrix} \quad (30)$$

According to the double closed-loop control of the battery converter is obtained and shown as:

$$\alpha v_{bat} = v_{dcref} + k_{ip1}(i_{batref} - i_{bat}) + k_{ii1} \int (i_{batref} - i_{bat}) dt \quad (31)$$

$$\frac{\partial \alpha v_{bat}}{\partial i_{bat}} = -k_{ip1} \quad (32)$$

In (31) and (32), k_{ip1} and k_{ii1} are the proportional and integral control parameters of the inner current loop for the battery converter, v_{dcref} is the rated DC bus voltage of DC microgrids, and i_{batref} is the rated current of the battery converter.

According to the power conservation principle and the control strategy for the SC converter, this is derived and shown as

$$i_{L1} = i_{SCref} = k_{vp2}(P_{scref} - i_{sc} v_{dc}) + k_{vi2} \int (P_{scref} - i_{sc} v_{dc}) dt \quad (33)$$

$$i_{sc} v_{dc} = i_{SC} v_{SC} \quad (34)$$

$$\frac{\partial i_{sc}}{\partial v_{dc}} = \frac{\partial \frac{i_{SC} v_{SC}}{v_{dc}}}{\partial v_{dc}} = \frac{-k_{vp2} i_{sc} v_{SC} v_{dc} - i_{SC} v_{SC}}{v_{dc}^2} \quad (35)$$

In (33) and (34), k_{vp2} and k_{vi2} are the proportional and integral control parameters of the outer power loop for the SC converter, P_{scref} is the reference power of the SC, and v_{SC} and i_{SC} are the actual voltage and current of the SC.

According to the third stability theorem, μ_1 is the minimum eigenvalue of $L^{-1/2}A_{ii}(i) L^{-1/2}$, and μ_2 is the minimum eigenvalue of $C^{-1/2}B_{vv}(v) C^{-1/2}$; μ_1 and μ_2 are obtained and shown as:

$$\mu_1 = \frac{k_{ip1} + \alpha R_1}{\alpha L_1} \quad (36)$$

$$\mu_2 = \frac{P_{DG} - k_{vp2} i_{sc} v_{SC} v_{dc} - i_{SC} v_{SC} - P_{load}}{C_{dc} v_{dc}^2} \quad (37)$$

Equation (14) is introduced into Equation (37) to obtain:

$$\mu_2 = \frac{P_{DG} - \frac{T}{T+T_S} (P_{sc-ref}(k) + \Delta P_{HESS}) (k_{vp2} v_{SC} + 1) - P_{load}}{C_{dc} v_{dc}^2} \quad (38)$$

According to the stability theorem in (19), the large-signal stability criterion for a DC microgrid with an HESS and CPLs is shown as:

$$\frac{k_{ip1} + \alpha R_1}{\alpha L_1} + \frac{P_{DG} - \frac{T}{T+T_S} (P_{sc-ref}(k) + \Delta P_{HESS}) (k_{vp2} v_{SC} + 1) - P_{load}}{C_{dc} v_{dc}^2} > 0 \quad (39)$$

To guarantee the large-signal stability of a DC microgrid, the criterion in (39) provides quantitative constraints on the CPL power, the filter inductor and capacitor, the DC bus voltage, the proportional control parameter (k_{ip1}) of the inner current loop for the battery converter and the proportional control parameter (k_{vp2}) of the outer power loop for the SC converter.

In islanded DC microgrids, when the CPL power increases, the system stability significantly deteriorates. Based on (39), regulating k_{ip1} and k_{vp2} of HESS converters during CPL power variations can easily achieve the large-signal stabilization of an islanded DC microgrid without extra equipment. The powers of the CPLs significantly vary during the working period and could also be regarded as dynamic loads at multiple time scales. The proposed large-signal stability criterion can analyze the transient state of dynamic loads.

Furthermore, when planning an islanded DC microgrid, the proposed large-signal stabilization method can improve the system large-signal stability; simultaneously, when the CPL power of an existing islanded DC microgrid significantly increases, the stabilization method can also guarantee large-signal stability.

The proposed procedure of the large-signal stability method for a DC microgrid with an HESS is expressed in Figure 11. Firstly, the control strategy for the HESS is proposed. The battery and the SC are controlled via PI double closed loops. The equivalent model of a DC microgrid is obtained according to the operating characteristics and control methods; then, the nonlinear model of a DC microgrid system is obtained based on mixed potential theory. The correctness of the mixed potential model is verified. When the mixed potential model is correct, the third stability theorem of the mixed potential theory is used to derive the large-signal stability criterion for DC microgrids. The control strategy for the HESS is considered in the criterion, and the control parameters are introduced into the large-signal stability criterion, which makes the criterion more accurate and comprehensive.

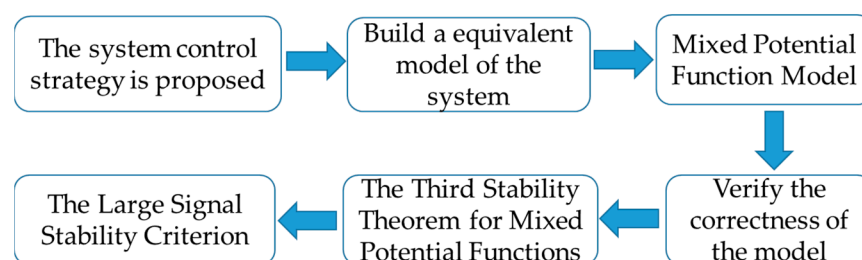


Figure 11. Procedure of large-signal stability method.

4. Large-Signal Stabilizations Method

The correctness of the large-signal stabilization method derived in (39) needs to be verified, and a typical islanded DC microgrid on the basis of Figure 2 is constructed using Matlab software. The system parameters are shown in Table 1. The CPLs are implemented via a closed-loop controlled DC/DC converter and a resistor. The islanded DC microgrid only operates in off-grid mode. When the powers between distributed generation and load are unbalanced, the hybrid energy storage system balances the powers. The platforms built in the experiments and simulations of this paper are both in island mode and are not connected to the grid.

Table 1. Simulation parameters of an islanded DC microgrid.

Parameter	Value
v_{dc} (V)	400
v_b (V)	150
v_{sc} (V)	160
v_{load} (V)	200
L_{bat} (mH)	5
L_s (mH)	20
C_{dc} (mF)	3
P_{CPL} (kW)	2
P_{DG} (kW)	4

1. In the simulation, the CPL power step causes a disturbance to the system. Two different groups of control parameters are designed and shown in Table 2. The control parameters of Group A satisfy (39), while the control parameters of Group B do not satisfy (39). The power variation of the CPLs is 2 kW to 12 kW. The load power variations are the same, while the control parameters of the hybrid energy storage system are different. Consequently, these groups are utilized to verify the stability influence of the control parameters of the hybrid energy storage system.

Table 2. Simulation parameters of A and B.

Parameter	A	B
k_{ip1}	10	2
k_{vp2}	0.1	0.1
P_{CPL}	2 kW \rightarrow 12 kW	
Satisfying the proposed large-signal stabilization method	Yes	No

When Group A is utilized, the waveforms of the CPL power step, DC bus voltage, battery power and SC power are shown in Figure 12. Obviously, when the initial CPL power is 2 kW, the DC bus voltage is 400 V, and the battery charging power is 2 kW. The DC microgrid is stable. As the CPL power increases from 2 kW to 12 kW, the DC bus voltage recovers to 400 V after a short fluctuation, and the battery changes from the charging state to the discharging state. At the same time, the SC quickly releases high-frequency power. Figure 12 indicates that the control parameters of Group A can guarantee the large-signal stability of a DC microgrid.

When Group B is utilized, the waveforms of the CPL power step, DC bus voltage, battery power and SC power are shown in Figure 13. Both CPL power and DC bus voltage strongly oscillate and cannot return to the steady state. The powers of the battery and SC are in a state of divergence. The battery cannot maintain a stable DC bus voltage. The DC microgrid is not stable during large disturbances. Figure 13 indicates that the control parameters of Group B cannot guarantee the large-signal stability of a DC microgrid.

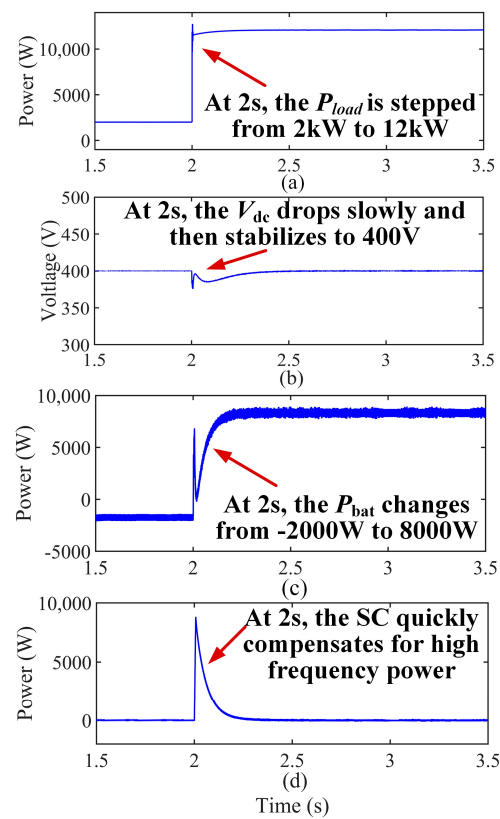


Figure 12. Simulation results when control parameters of Group A are used. (a) CPL power, (b) DC bus voltage, (c) battery power and (d) SC power.

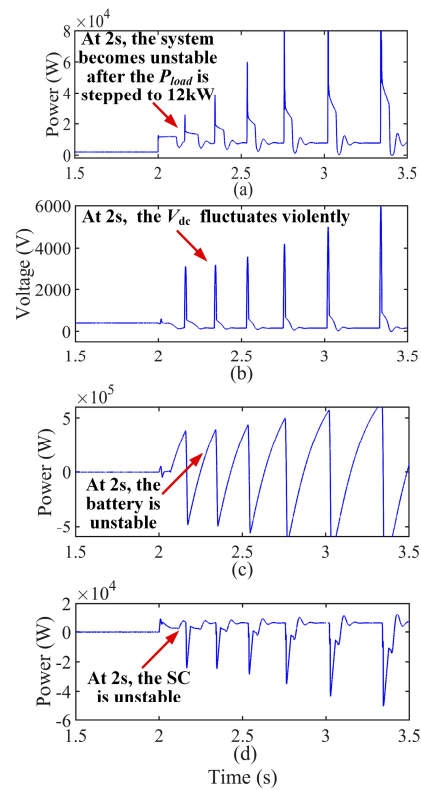


Figure 13. Simulation results when control parameters of Group B are used. (a) CPL power, (b) DC bus voltage, (c) battery power and (d) SC power.

Figures 12 and 13 verify the validity of the derived large-signal stability criterion. The system is stable when the system control parameters satisfy the proposed criterion, otherwise the system is unstable. The results also illustrate that the large-signal stability of an islanded DC microgrid can be improved by regulating the proportional control parameters of the battery converter and SC converter.

2. Based on (39), the large-signal stability of an islanded DC microgrid also closely relates to CPL power. When the control parameters of the HESS converters are the same, two large power variations of the CPLs are introduced, as shown in Table 3. The control parameters of the energy storage system are the same, but the load power variations are different. The stability influence of the load power variations is verified, and the allowable load power variations are determined.

Table 3. Simulation parameters of Groups C and D.

Parameter	C	D
k_{ip1}		8.0
k_{vp2}		0.1
P_{CPL}	2 kW \rightarrow 8 kW	2 kW \rightarrow 12 kW
Satisfying the proposed large-signal stabilization method	Yes	No

When Group C is utilized, the waveforms of the CPL power step, DC bus voltage, battery power and SC power are shown in Figure 14. At 2 s, the CPL power increases from 2 kW to 8 kW; the DC bus voltage recovers to 400 V after a short decrease; and the battery changes from the charging state to the discharging state. Simultaneously, the SC quickly releases high-frequency power. Figure 14 indicates that the large-signal stability of a DC microgrid can be guaranteed during the large disturbance of Group C.

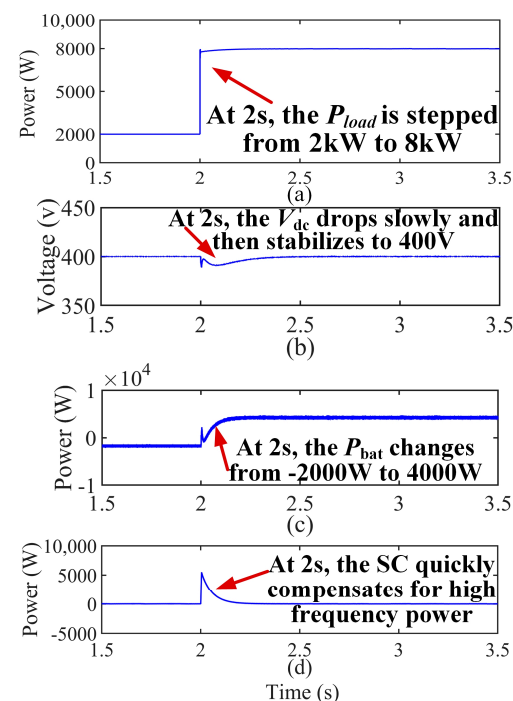


Figure 14. Simulation results when control parameters of Group C are used. (a) CPL power, (b) DC bus voltage, (c) battery power and (d) SC power.

When Group D is utilized, the waveforms of the CPL power step, DC bus voltage, battery power and SC power are shown in Figure 15. After the large disturbance, both CPL power and DC bus voltage have serious oscillations and cannot return to the steady state.

The powers of the battery and SC are unstable. The battery cannot maintain a stable DC bus voltage. The DC microgrids are not stable during large disturbances. It can be seen from Figure 15 that the large-signal stability of a DC microgrid cannot be guaranteed under the large disturbance of Group D.

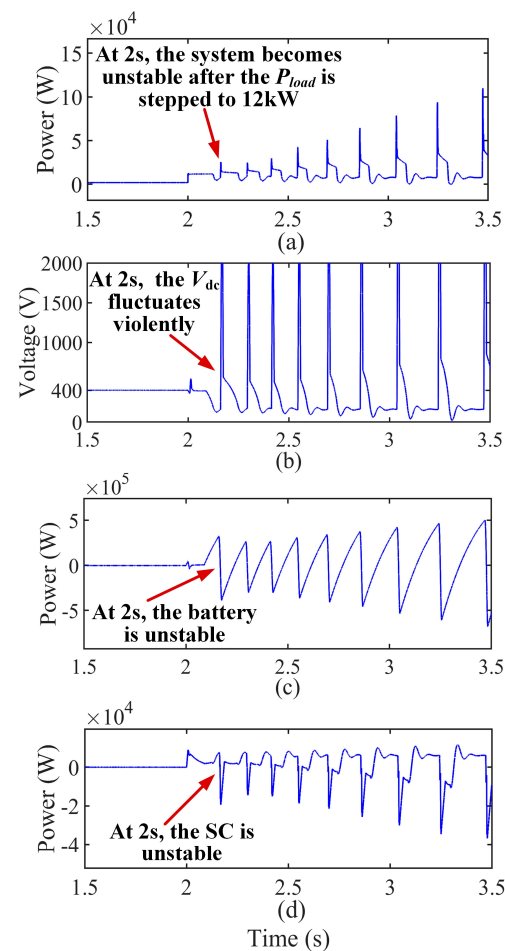


Figure 15. Simulation results when control parameters of Group D are used. (a) CPL power, (b) DC bus voltage, (c) battery power and (d) SC power.

Figures 14 and 15 also verify the correctness of the derived large-signal stability criterion and show that the large-signal stability of an islanded DC microgrid closely relates to large disturbances.

The simulation results indicate that the large-signal stabilization method for islanded DC microgrids in (39) is correct and also show that regulating the proportional control parameters of the SC converter and the battery converter can significantly improve the large-signal stability of islanded DC microgrids.

5. Experimental Results

The effectiveness of the proposed large-signal stability method for islanded DC microgrids is verified. This paper builds the experimental platform based on Figure 2, as shown in Figure 16. The experimental platform includes a DC power supply, the battery and the bidirectional DC/DC converter, the SC and the bidirectional DC/DC converter, and the CPLs. The parasitic inductance of the resistor used for the load step is also measured, as shown in Table 4. The experimental parameters are shown in Table 5. The supercapacitor is an electric double-layer capacitor, which is composed of two supercapacitors connected in series. The capacity of each supercapacitor is 166 F, and the rated voltage is 24 V.

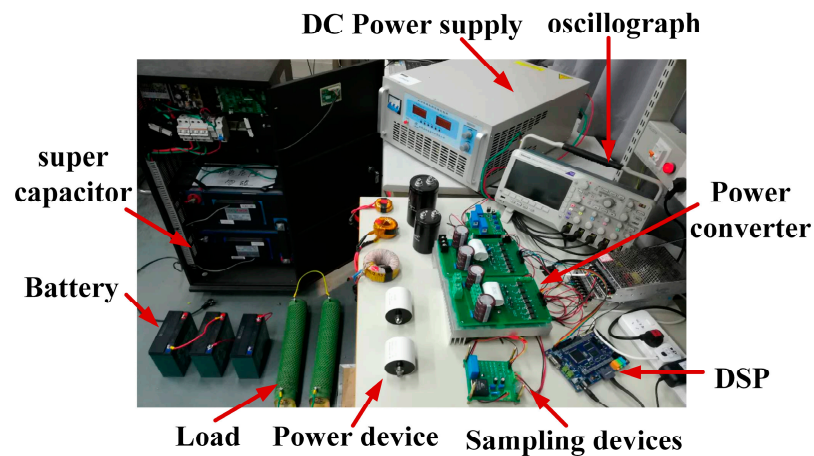


Figure 16. DC microgrid experimental platform.

Table 4. Parasitic inductance value of resistive load.

Load Resistance (Ω)	Inductance Value (mH)
100	1.3
28.6	0.4
20	0.28

Table 5. Parameters of experimental platform.

Parameter	Value
v_{dc} (V)	60
v_b (V)	36
v_{sc} (V)	24
v_{load} (V)	48
L_1 (mH)	2.95
L_2 (mH)	5
L_3 (mH)	5
C_{dc} (mF)	2.2

Large disturbances are introduced via power variations of the CPLs. Two groups with different control parameters are designed. The parameters of Group E satisfy (39), while the parameters of Group F do not satisfy (39), and shown in Table 6. The power variations of the CPLs are from 23 W to 80 W. In Group E and Group F, the load power variations are the same, and the control parameters of the energy storage system are different, to verify the stability of the influence of the control parameters of the hybrid energy storage system.

Table 6. Experimental parameters of Groups E and F.

Parameter	E	F
k_{ip1}	0.6	0.2
k_{vp2}	0.1	0.1
P_{CPL}	23 W \rightarrow 80 W	
Satisfying the proposed large-signal stabilization method	Yes	No

When Group E is adopted, the waveforms of the DC bus voltage, CPL current, and battery and SC currents are shown in Figure 17. The CPL power increases from 23 W to 80 W, and the DC bus voltage slightly decreases. Simultaneously, the SC responds rapidly, and the output current of the SC instantaneously increases. While the battery current gradually increases, the current of the SC tends to be zero. Obviously, the DC microgrid maintains stable operation during large disturbances.

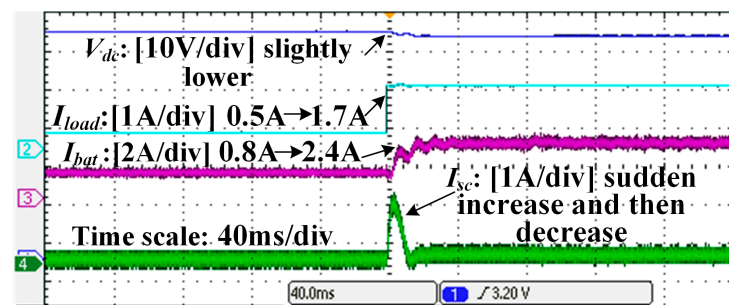


Figure 17. Control parameters of Group E: DC bus voltage, CPL current, battery current and SC current of a DC microgrid.

When Group F is utilized, the DC bus voltage, CPL current, and battery and SC currents are shown in Figure 18. After the same CPL power variation, the DC bus voltage slightly decreases; the battery current violently fluctuates; and the SC current also fluctuates near zero. Figure 18 shows that the DC microgrid is unstable during large disturbances.

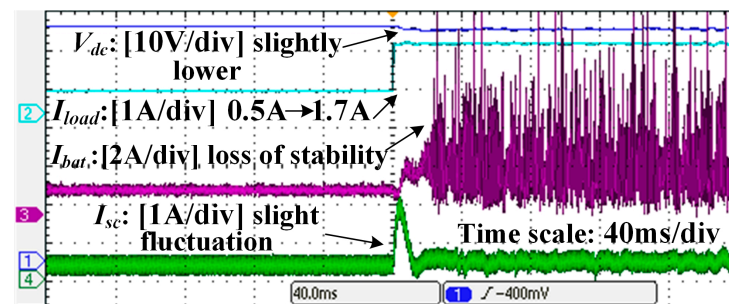


Figure 18. Control parameters of Group F: DC bus voltage, CPL current, battery current and SC current of a DC microgrid.

The comparison between Figures 17 and 18 illustrates that when the control parameters satisfy the derived large-signal stabilization method in (39), the DC microgrid can remain stable under large disturbances. Conversely, when the control parameters do not satisfy (39), the DC microgrid cannot achieve large-signal stability. The experimental results verify the effectiveness of the proposed criterion. The results also illustrate that the proposed large-signal stability method for islanded DC microgrids can be improved by regulating the proportional control parameters of the battery converter and SC converter.

Similarly, based on (39), the large-signal stability of an islanded DC microgrid closely relates to CPL power. In Group G and Group H, the control parameters of the hybrid energy storage system are the same, but the load power steps are different, as shown in Table 7. The disturbances of Group G are from 23 W to 80 W, satisfying (39), while the disturbances of Group H are from 23 W to 115 W, not satisfying (39).

Table 7. Experimental parameters of G and H.

Parameter	G	H
k_{ip1}		0.4
k_{vp2}		0.1
P_{CPL}	23 W \rightarrow 80 W	23 W \rightarrow 115 W
Satisfying the proposed large-signal stabilization method	Yes	No

When Group G is used, the DC bus voltage, CPL current, battery current and SC current of the DC microgrid are shown in Figure 19. When the CPL power increases from 23 W to 80 W, the DC bus voltage slightly decreases. At the same time, the SC rapidly

discharges, and the battery current slowly increases. Obviously, after the power step of the CPLs, the DC microgrid maintains a new stable state.

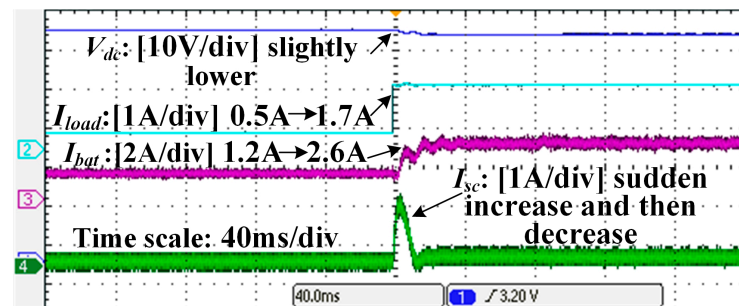


Figure 19. Control parameters of Group G: DC bus voltage, CPL current, battery current and SC current of a DC microgrid.

When Group H is applied, the DC bus voltage, CPL current, battery current and SC current of the DC microgrid are shown in Figure 20. Unfortunately, after the CPL power increases, the DC bus voltage significantly drops; the battery current seriously fluctuates from 0.4 A to 6 A, and the SC current also fluctuates in a small range. Consequently, the DC microgrid is unstable during large disturbances.

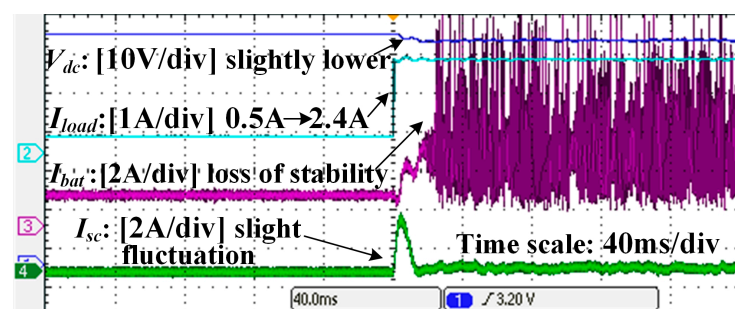


Figure 20. Control parameters of Group H: DC bus voltage, CPL current, battery current and SC current of a DC microgrid.

Figures 19 and 20 also verify the correctness of the derived large-signal stability criterion. When the load power variations satisfy the criterion, the system is stable, otherwise the system is unstable. This shows that the criterion proposed in this paper can constrain the variation of load power.

In the experimental results shown in Figures 17–20, the green waveform is the current waveform of the supercapacitor. It can be concluded that the supercapacitor quickly charges and discharges to absorb or release high-frequency-power fluctuations.

The experimental results indicate that under the same disturbance, regulating the proportional control parameters of the battery converter and SC converter can significantly improve the large-signal stability of an islanded DC microgrid. The simulation results coincide with the experimental results, and all results indicate that the large-signal stabilization method for islanded DC microgrids in (39) is correct.

6. Conclusions

For an islanded DC microgrid constituted of an HESS, CPLs and DGs, this paper presents a large-signal stabilization method. Firstly, the topological structure of and control strategy for a DC microgrid is proposed. According to the dynamic characteristics of the DGs, the HESS and the CPLs, the nonlinear model of the system is obtained. Then, the large-signal model and large-signal stability criterion for a DC microgrid are obtained using mixed potential functions and the stability theorem. A large-signal stabilization method is

proposed, and the CPL power, the filter inductor and capacitor, the DC bus voltage, the proportional control parameter (k_{ip1}) of the inner current loop for the battery converter and the proportional control parameter (k_{vp2}) of the outer power loop for the SC converter are all considered. Furthermore, the regulating control parameters of HESS converters can easily achieve the large-signal stabilization of an islanded DC microgrid without extra equipment. The experimental and simulation results verify the correctness of the proposed large-signal stabilization method for islanded DC microgrids.

Author Contributions: Study design, Literature search and Manuscript writing, X.L.; Graph production, Data analysis and Data processing, Y.S.; Supervision and Data collection, X.S.; Resources, and Writing—review and editing, J.Z.; Translation and Literature search, Y.Q. All authors have read and agreed to the published version of the manuscript.

Funding: National Key R & D Program of China: 2021YFE0103800.

Conflicts of Interest: The authors declare no conflict of interest.

References

1. Liang, D.; Qin, C.; Wang, S.; Guo, H. Reliability evaluation of DC distribution power network. In Proceedings of the 2018 China International Conference on Electricity Distribution (CICED), Tianjin, China, 17–19 September 2018; pp. 654–659.
2. Zhang, Q.J.; Zeng, Y.J.; Liu, Y.C.; Zhuang, X.Z.; Zhang, H.W.; Hu, W.B.; Guo, H.H. An Improved Distributed Cooperative Control Strategy for Multiple Energy Storages Parallel in Islanded DC Microgrid. *IEEE J. Emerg. Sel. Top. Power Electron.* **2022**, *10*, 455–468. [\[CrossRef\]](#)
3. Haruni, A.M.O.; Negnevitsky, M.; Haque, E.; Gargoom, A. A Novel Operation and Control Strategy for a Standalone Hybrid Renewable Power System. *IEEE Trans. Sustain. Energy* **2013**, *4*, 402–413. [\[CrossRef\]](#)
4. Chen, X.; Shi, M.; Zhou, J.; Chen, Y.; Zuo, W.; Wen, J.; He, H. Distributed Cooperative Control of Multiple Hybrid Energy Storage Systems in a DC Microgrid Using Consensus Protocol. *IEEE Trans. Ind. Electron.* **2020**, *67*, 1968–1979. [\[CrossRef\]](#)
5. Thang, T.V.; Ahmed, A.; Kim, C.-I.; Park, J.-H. Flexible System Architecture of Stand-Alone PV Power Generation with Energy Storage Device. *IEEE Trans. Energy Convers.* **2015**, *30*, 1386–1396. [\[CrossRef\]](#)
6. Tin, B.; Sandor, I.; Damir, S. Model predictive direct current control of a permanent magnet synchronous generator based on flexible Lyapunov function considering converter dead time. *IEEE Trans. Ind. Appl.* **2018**, *54*, 2899–2912.
7. Tahim, A.P.N.; Pagano, D.J.; Lenz, E.; Stramosk, V. Modeling and Stability Analysis of Islanded DC Microgrids Under Droop Control. *IEEE Trans. Power Electron.* **2015**, *30*, 4597–4607. [\[CrossRef\]](#)
8. Chen, S.; Yang, Q.; Zhou, J.; Chen, X. A model predictive control method for hybrid energy storage systems. *CSEE J. Power Energy Syst.* **2021**, *7*, 329–338.
9. Peng, Q.; Yuan, Z.; Ouyang, B.; Guo, P.; Qu, L. Research on the Optimal Operation Method of DC Microgrid Base on the New DC Power Distribution Management System. *Electronics* **2019**, *9*, 9. [\[CrossRef\]](#)
10. Pirooz, A.; Noroozian, R. Model predictive control of classic bidirectional dc-dc converter for battery applications. In Proceedings of the 2016 7th Power Electronics and Drive Systems Technologies Conference (PEDSTC), Tehran, Iran, 16–18 February 2016; pp. 517–522.
11. Khomenko, M.; Veligorskyi, O.; Husev, O.; Tytelmaier, K.; Yershov, R. Model predictive control of photovoltaic bidirectional DC-DC converter with coupled inductors. In Proceedings of the 2017 IEEE First Ukraine Conference on Electrical and Computer Engineering (UKRCON), Kyiv, Ukraine, 29 May–2 June 2017; pp. 578–583.
12. Xiao, J.; Wang, P.; Setyawan, L. Multilevel Energy Management System for Hybridization of Energy Storages in DC Microgrids. *IEEE Trans. Smart Grid* **2016**, *7*, 847–856. [\[CrossRef\]](#)
13. Lin, P.; Zhao, T.; Wang, B.; Wang, Y.; Wang, P. A Semi-Consensus Strategy Toward Multi-Functional Hybrid Energy Storage System in DC Microgrids. *IEEE Trans. Energy Convers.* **2020**, *35*, 336–346. [\[CrossRef\]](#)
14. Oliveira, T.R.; Silva, W.W.A.G.; Donoso-Garcia, P.F. Distributed Secondary Level Control for Energy Storage Management in DC Microgrids. *IEEE Trans. Smart Grid* **2017**, *8*, 2597–2607. [\[CrossRef\]](#)
15. Zhang, M.; Xu, Q.; Zhang, C.; Nordström, L.; Blaabjerg, F. Decentralized Coordination and Stabilization of Hybrid Energy Storage Systems in DC Microgrids. *IEEE Trans. Smart Grid* **2022**, *13*, 1751–1761. [\[CrossRef\]](#)
16. Ramos, G.A.; Costa-Castelló, R. Energy Management Strategies for Hybrid Energy Storage Systems Based on Filter Control: Analysis and Comparison. *Electronics* **2022**, *11*, 1631. [\[CrossRef\]](#)
17. Feng, L.; Zhang, J.; Li, G.; Zhang, B. Cost reduction of a hybrid energy storage system considering correlation between wind and PV power. *Prot. Control Mod. Power Syst.* **2016**, *1*, 11. [\[CrossRef\]](#)
18. Yang, F.; Xue, H.; Wang, Y.F. Research on Control Strategy of Supercapacitors Energy Storage System. *Adv. Mater. Res.* **2011**, *347–353*, 3881–3885. [\[CrossRef\]](#)
19. Du, W.; Zhang, J.; Zhang, Y.; Qian, Z. Stability Criterion for Cascaded System With Constant Power Load. *IEEE Trans. Power Electron.* **2013**, *28*, 1843–1851. [\[CrossRef\]](#)

20. Cespedes, M.; Xing, L.; Sun, J. Constant-Power Load System Stabilization by Passive Damping. *IEEE Trans. Power Electron.* **2011**, *26*, 1832–1836. [\[CrossRef\]](#)
21. Rahimi, A.M.; Emadi, A. Active Damping in DC/DC Power Electronic Converters: A Novel Method to Overcome the Problems of Constant Power Loads. *IEEE Trans. Ind. Electron.* **2009**, *56*, 1428–1439. [\[CrossRef\]](#)
22. Magne, P.; Marx, D.; Nahid-Mobarakeh, B.; Pierfederici, S. Large-Signal Stabilization of a DC-Link Supplying a Constant Power Load Using a Virtual Capacitor: Impact on the Domain of Attraction. *IEEE Trans. Ind. Appl.* **2012**, *48*, 878–887. [\[CrossRef\]](#)
23. Zhang, X.; Ruan, X.; Zhong, Q.C. Improving the stability of cascaded DC/DC converter systems via shaping the input impedance of the load converter with a parallel or series virtual impedance. *IEEE Trans. Ind. Electron.* **2015**, *62*, 7499–7512. [\[CrossRef\]](#)
24. Zhao, Y.; Qiao, W.; Ha, D. A sliding-mode duty-ratio controller for dc/dc buck converters with constant power loads. *IEEE Trans. Ind. Appl.* **2014**, *50*, 1448–1458. [\[CrossRef\]](#)
25. Xu, Q.; Zhang, C.; Wen, C.; Wang, P. A Novel Composite Nonlinear Controller for Stabilization of Constant Power Load in DC Microgrid. *IEEE Trans. Smart Grid* **2019**, *10*, 752–761. [\[CrossRef\]](#)
26. Gui, Y.; Han, R.; Guerrero, J.M.; Vasquez, J.C.; Wei, B.; Kim, W. Large-Signal Stability Improvement of DC-DC Converters in DC Microgrid. *IEEE Trans. Energy Convers.* **2021**, *36*, 2534–2544. [\[CrossRef\]](#)
27. Vafamand, N.; Yusefizadeh, S.; Khooban, M.H.; Bendtsen, J.D.; Dragicevic, T. Adaptive TS Fuzzy-Based MPC for DC Microgrids With Dynamic CPLs: Nonlinear Power Observer Approach. *IEEE Syst. J.* **2019**, *13*, 3203–3210. [\[CrossRef\]](#)
28. Guo, L.; Feng, Y.B.; Li, X.L. Study on stability analysis and damping control method of DC microgrid. In Proceedings of the 2018 IEEE 2nd International Electrical and Energy Conference (CIEEC), Beijing, China, 4–6 November 2018; Volume 36, pp. 927–936.
29. Kollimalla, S.K.; Mishra, M.K.; Ukil, A.; Gooi, H.B. DC Grid Voltage Regulation Using New HESS Control Strategy. *IEEE Trans. Sustain. Energy* **2017**, *8*, 772–781. [\[CrossRef\]](#)
30. Zhao, Z.L.; Yang, P.; Zheng, C.L. Review on dynamic stability research of microgrid. *Trans. China Electrotech. Soc.* **2017**, *32*, 111–122.
31. Anand, S.; Fernandes, B.G. Reduced-Order Model and Stability Analysis of Low-Voltage DC Microgrid. *IEEE Trans. Ind. Electron.* **2013**, *60*, 5040–5049. [\[CrossRef\]](#)
32. Zekun, L.; Wei, P.; Li, K. Large-disturbance Stability Analysis of DC Microgrid with Constant Power Load and its Transient Voltage Stability Control Strategy. In Proceedings of the 2018 China International Conference on Electricity Distribution (CICED), Tianjin, China, 17–19 September 2018; pp. 1686–1690.
33. Marx, D.; Magne, P.; Nahid-Mobarakeh, B.; Pierfederici, S.; Davat, B. Large Signal Stability Analysis Tools in DC Power Systems With Constant Power Loads and Variable Power Loads—A Review. *IEEE Trans. Power Electron.* **2012**, *27*, 1773–1787. [\[CrossRef\]](#)
34. Sanchez, S.; Molinas, M. Large Signal Stability Analysis at the Common Coupling Point of a DC Microgrid: A Grid Impedance Estimation Approach Based on a Recursive Method. *IEEE Trans. Energy Convers.* **2015**, *30*, 122–131. [\[CrossRef\]](#)
35. Xie, W.; Han, M.; Cao, W.; Guerrero, J.M.; Vasquez, J.C. System-Level Large-Signal Stability Analysis of Droop-Controlled DC Microgrids. *IEEE Trans. Power Electron.* **2021**, *36*, 4224–4236. [\[CrossRef\]](#)
36. Du, W.J.; Zhang, J.M.; Qian, Z.M. Compensation methodology for DC bus voltage of cascaded system formed by Buck converters. *Trans. China Electrotech. Soc.* **2015**, *30*, 135–142.
37. Hassan, M.A.; Li, E.-p.; Li, X.; Li, T.; Duan, C.; Chi, S. Adaptive Passivity-Based Control of DC-DC Buck Power Converter with Constant Power Load in DC Microgrid Systems. *IEEE J. Emerg. Sel. Top. Power Electron.* **2019**, *7*, 2029–2040. [\[CrossRef\]](#)
38. Huang, M.; Ji, H.; Sun, J.; Wei, L.; Zha, X. Bifurcation-Based Stability Analysis of Photovoltaic-Battery Hybrid Power System. *IEEE J. Emerg. Sel. Top. Power Electron.* **2017**, *5*, 1055–1067. [\[CrossRef\]](#)
39. Peng, D.; Huang, M.; Li, J.; Sun, J.; Zha, X.; Wang, C. Large-Signal Stability Criterion for Parallel-Connected DC-DC Converters With Current Source Equivalence. *IEEE Trans. Circuits Syst. II Express Briefs* **2019**, *66*, 2037–2041. [\[CrossRef\]](#)
40. Zhang, Z.; Yang, X.; Zhao, S.; Wu, D.; Cao, J.; Gao, M.; Zeng, G.; Wang, Z. Large-signal stability analysis of islanded DC microgrids with multiple types of loads. *Int. J. Electr. Power Energy Syst.* **2022**, *143*, 108450. [\[CrossRef\]](#)
41. Xie, W.; Han, M.; Cao, W.; Guerrero, J.M.; Vasquez, J.C. Virtual Resistance Tradeoff Design for DCMG Grid-Forming Converters Considering Static- and Large-Signal Dynamic Constraints. *IEEE Trans. Power Electron.* **2021**, *36*, 5582–5593. [\[CrossRef\]](#)
42. Wang, S.; Yu, Y.; Tian, Z.; Zha, X. Energy-based large-signal stability analysis of DC microgrid considering dynamic interactions between multiple converters. In Proceedings of the 2021 IEEE 16th Conference on Industrial Electronics and Applications (ICIEA), Chengdu, China, 1–4 August 2021; pp. 1032–1039.
43. Zakir, M.; Sher, H.A.; Arshad, A.; Lehtonen, M. A fault detection, localization, and categorization method for PV fed DC-microgrid with power-sharing management among the nano-grids. *Int. J. Electr. Power Energy Syst.* **2022**, *137*, 107858. [\[CrossRef\]](#)